Spray Cooling Modeling: Droplet Impact and Vapor Growth Effects on Heat Transfer in Micro & Macro-Gravity

R. Paneer Selvam[1, 2], Matthew Hamilton[1, 2], Eric A. Silk[3]

[1]*Power Electronic Leveling Solutions, 700 W. Research Boulevard, Fayetteville, AR 72701*
[2]*Computational Mechanics Lab, BELL 4190 University of Arkansas, Fayetteville, AR 72701,*
email: rps@uark.edu, phone: 479-575-5356
[3]*NASA Goddard Space Flight Center, Greenbelt, MD 20771*

Abstract: In recent years spray cooling has established itself as a novel solution for high heat flux applications. As the need for thermal management of high power density electronic systems (lasers, radars, etc) grows, interest in spray cooling as a solution to thermal management issues on space based platforms is increasing. The aim of this investigation is to explore the effects of gravity on spray cooling heat transfer. The effect of micro and macro gravity on spray cooling heat transfer as well as the effect of droplet impact on vapor bubble growth and development are investigated. A 2-D multiphase flow computer model has been developed. The model includes surface tension effects, viscosity, phase change, and gravity. The interface between the liquid and the vapor is modeled using the level set method. The liquid film (FC-72) impacted by the droplet has been approximated as 40μm thick. The corresponding wall heat transfer during droplet impingement is computed for gravitational constants ranging 0.0001g to 2g. For comparison purposes, simulations of vapor bubble growth in the macro-region of (1 mm to 10 mm normal to the wall) has also been reported for model verification. The computed Nusselt number versus time is presented as a function of temperature contours and velocity.

1. Introduction

Spray cooling has been a topic of interest since the mid-1970s (Cabrera and Gonzalez 2003). It is a heat transfer technique that has been used in industry for many years (i.e. foundry metal quenching) and has a proven capability at high heat flux heat removal (upwards of 100 W/cm^2 with fluorinerts and 1000 W/cm^2 using water). Several experiments dedicated to gaining a better understanding of the spray cooling process have been conducted in recent years (Yang et al., 1996; Chow et al., 1997; Lin and Ponnappan, 2003; Mudawar, 2001; Pautsch and Shedd, 2005; Rowden et al.; 2006). However, despite its common usages and experimental studies dedicated to it, a theoretical understanding of spray cooling phenomena and the heat transfer mechanisms associated with it has yet to be attained. Nonetheless, understanding of the process is of critical importance in the future design and implementation of spray cooling heat transfer systems. This is due to the highly complex interaction of the thin liquid film, liquid droplet impact at the liquid/vapor interface, and phase-change in the liquid film, as shown in figure 1.

While each of these effects has been investigated individually, a comprehensive study of their overall impact on one another is still needed. Due to the highly non-linear nature of most multiphase systems and the spray cooling process itself there are two techniques available for the determination of spray cooling heat flux: computer modeling and direct experimentation. The current work uses a computer modeling approach. While this work is not intended to provide a comprehensive solution at this time, it is considered a step in the solution process.

A detailed review of the current literature on computer modeling of spray cooling and methods to solve multiphase flow problems is presented in Selvam et al. (2005). Recent studies

by Selvam and Ponnappan (2004),and Selvam et al.(2005) have concluded that computer modeling of nucleate boiling in a thin liquid film (≈70 μm) experiencing droplet impingement will provide valuable information regarding the design of future spray cooling experiments. In the study by Pautsch et al.(2004), a variation of the liquid film thickness under the spray region was observed. These variations in liquid film thickness ranged from 42μm to 162μm under the spray region with a maximum thickness of 396μm found in the die corners. In the present study, a film thickness of 73.6μm was used, similar to the results directly under the spray. Previous computational efforts detailing the growing of a vapor bubble in a thin liquid film and the transient wall heat transfer associated with it were reported by Selvam et al.(2005a). Continuation studies of this simplified problem emphasized heat transfer due to bubble growth and bursting (Selvam et al. 2005b) as well as the impact of droplet impingement on growing bubbles (Selvam et al. 2005c). The authors determined that an impinging droplet had a much higher heat transfer, due to transient conduction associated with the bubble growth process.

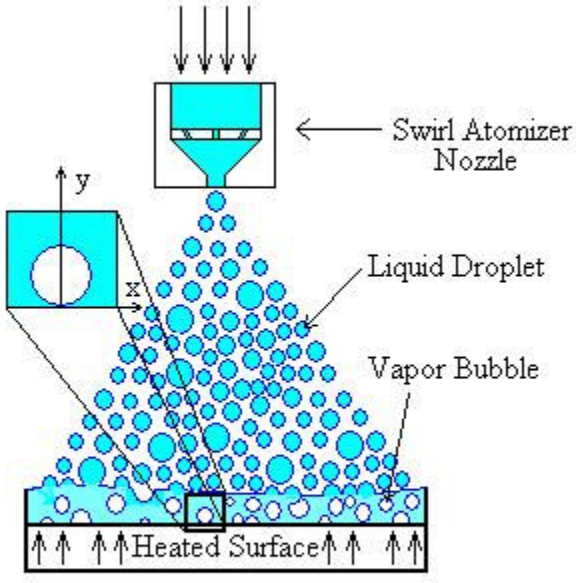

Fig. 1: Spray Cooling

Dhir et al. (1998) and Qiu and Dhir (2002) performed work on microgravity effects on nucleate boiling. Dhir et al. (1998) noted that bubbles grown at reduced gravity grew larger and had correspondingly longer growth periods, and grew in the shape of an oblong sphere. With the model Dhir et al. developed, bubble lift-off diameters were determined. For 1g, the bubble grows to a diameter 2.3mm and then detaches from the hot surface whereas in the microgravity environment the bubble grows to a diameter of 210mm before detaching. Hunnell et al.(2006) performed experiments on microgravity effects on spray cooling. Using a ground-based horizontal spray configuration to simulate reduced gravity, they determined that little difference was apparent between vertical configuration (gravity) and horizontal (microgravity). They do suggest that this result may instead indicate that the horizontal configuration cannot adequately simulate reduced gravity. The current study is a continuation of Rowden et al. (2006), who modeled spray cooling and found that significant differences between varying gravitational constants were not observed when using a 44μm thick liquid film. The current study extends the initial investigation by Rowden et al. (2006) by investigating bubble growth in the liquid film thickness as well as an increased film thickness. The gravity effect on heat transfer due to droplet

impingement and vapor bubble growth is also detailed. The effect of gravitational variations on heat transfer phenomena in spray cooling is a prime consideration for the feasibility and applicability of spray cooling systems in such environments. In order to determine the mechanisms governing heat transfer in microgravity environments, a larger simulation was computed in order to determine the effect of scale on gravitational variation.

2. Numerical formulation for multiphase flow using level set method

A review of numerical modeling techniques applied to multiphase flows can be found in Selvam et al. (2005). In the present effort, the level set method two-phase flow model introduced by Sussman et al.(1994) for bubble dynamics was used. This model was modified by Son and Dhir (1998) and later by Son et al.(2002) for modeling vapor bubble growth due to phase change. In their work, the phases are defined as a positive or negative distance from the interface given by a function φ. A positive sign is used for the liquid phase and a negative sign for the vapor phase. For more information on the level set method and its applications, see the works of Sethian (1999) and/or Osher and Fedikiw (2003). These texts provide extensive application examples of the level set method in various areas of science and engineering.

2.1 Governing equations

In the present model, the fluid properties including density, viscosity and thermal conductivity are held constant for both phases. The flow is assumed to be incompressible. The Navier-Stokes equations used are as follows:

$$\rho(\partial_t \mathbf{u} + \mathbf{u}.\nabla \mathbf{u}) = -\nabla p + \rho \mathbf{g} - \sigma\kappa\nabla H + \nabla.\mu\nabla \mathbf{u} + \nabla.\mu\nabla \mathbf{u}^T \quad (1)$$

$$\rho c_{pl}(\partial_t T + \mathbf{u}.\nabla T) = \nabla.k\nabla T \quad \text{for } H>0 \text{ and } T=T_{sat}(p_v) \text{ for } H = 0 \quad (2)$$

$$\nabla.\mathbf{u} = \mathbf{m}.\nabla\rho/\rho^2 \quad (3)$$

$$\text{where : } \rho = \rho_v + (\rho_l - \rho_v)H. \quad (4)$$

These governing equations incorporate the effects of surface tension, gravity and phase change at the interface. The value of μ and k are calculated using a relation similar to Eq. (4). Here:

$$\begin{aligned} H &= 1 \text{ if } \varphi \geq 1.5h \\ &= 0 \text{ if } \varphi \leq -1.5h \\ &= 0.5 + \varphi/(3h) + \sin[2\pi\varphi/(3h)]/(2\pi) \text{ if } |\varphi| \leq 1.5h \end{aligned} \quad (5)$$

The grid spacing is h. The Eq. (5) implies that the interface separating two phases is replaced by a transition region of finite thickness. The volume source term included in the continuity equation (3) due to liquid-vapor phase change is derived from the conditions of mass continuity and energy balance at the interface:

$$m = \rho(\mathbf{u}_{int} - \mathbf{u}) = k\nabla T/h_{fg} \quad (6)$$

In the level set formulation, the level set function φ, is advanced and reinitialized as according to the following:

$$\partial_t \varphi = - \mathbf{u}_{int} . \nabla \varphi \tag{7}$$

$$\partial_t \varphi = \varphi_o (1- |\nabla \varphi|) /\sqrt{(\varphi_o^2 + h^2)} \tag{8}$$

where φ_o is a solution of Eq. (7). The surface tension effect is considered in the momentum equation by using a step function H (H=0 in the vapor and 1 in the liquid) and κ is the interfacial curvature expressed as:

$$\kappa = \nabla . (\nabla \varphi/|\nabla \varphi|) \tag{9}$$
$$= (\varphi_y^2 \varphi_{xx} - 2 \varphi_x \varphi_y \varphi_{xy} + \varphi_x^2 \varphi_{yy})/(\varphi_x^2 + \varphi_y^2)^{3/2} \text{ for 2D}$$

Here the subscripts denote differentiation with respect to φ. The surface tension force ($- \sigma\kappa\nabla H$) is implemented in the volume form to avoid the need for explicit description of the interface as suggested by Brackbill et al.(1992).

2.2 Nondimensional form of the governing equations

The nondimensional form of the above governing equations was derived using a characteristic length (l_r), velocity (u_r), time (t_r), and temperature (T^*). The definition for each of these terms is shown in eqns 10a through 10c. These values were defined in a similar manner to the convention in the works by Son and Dhir (1998) and Selvam et al.(2004). These reference

$$l_r=\sqrt{\sigma/g(\rho_l-\rho_v)} \tag{10a}$$

$$u_r=\sqrt{gl_r},\ tr=l_r/u_r \tag{10b}$$

$$T^*=(T-T_{sat})/(T_w-T_{sat}) \tag{10c}$$

values are chosen so that the Bond number equals 1 and the Weber number is slightly greater than 1. For the baseline gravity case ($g_y = 1$), the Froude number also equals 1. If ρ, k, μ, and c_p of the liquid are also taken as reference values, the governing equations (Eq. 1-4) can be nondimensionalized, and without superscripts become:

$$\rho(\partial_t \mathbf{u} + \mathbf{u}. \nabla \mathbf{u}) = -\nabla p + \rho g_y / Fr^2 - \kappa\nabla H/We + (\nabla.\mu\nabla \mathbf{u} + \nabla.\mu\nabla \mathbf{u}^T)/Re \tag{11}$$

$$\rho c_{pl}(\partial_t T + \mathbf{u}. \nabla T) = (\nabla.k\nabla T)/Pe \quad \text{for } H>0 \tag{12}$$

$$\nabla . \mathbf{u} = Ja\ k\ \nabla T . \nabla\rho/ (Pe\ \rho^2) \tag{13}$$

$$\mathbf{u}_{int} = \mathbf{u} + Ja\ k\ \nabla T/ (Pe\ \rho) \tag{14}$$

where:

$$\mathrm{Re} = \frac{\rho_l u_r l_r}{\mu_l},\quad We = \frac{\rho_l u_r^2 l_r}{\sigma},\quad Ja = \frac{c_{pl}\Delta T}{h_{fg}},\quad Fr = \frac{u_r}{\sqrt{g l_r}},\quad \mathrm{Pr} = \frac{c_{pl}\mu_l}{k_l},\quad Pe = \mathrm{Re}\,\mathrm{Pr} = \frac{\rho_l u_r l_r c_{pl}}{k_l}$$

In the following equations (Eq. 11-14), ρ, k, μ, and c_p are taken as dimensionless with respect to the reference values. The variable g_y is the gravitational force in the y-direction. To reflect the gravitational-constant's variation from 2.0g to 0.0001g, the square of the Froude number (Fr) will be varied from 10,000 for the 0.0001g case to 0.5 for the 2g case.

2.3 Boundary conditions

The boundary conditions for the governing equations are shown in Fig. 2 and also given below:

At the wall (y=0): $u = v = 0$, $T = T_w$, $\varphi_y = 0$.
At the planes of symmetry (x=0 and $x = x_{max}$): $u = v_x = T_x = \varphi_x = 0$.
At the top of the computational domain (free surface, $y = y_{max}$): $u_y = v_y = \varphi_y = 0$, $T = T_{sat}$

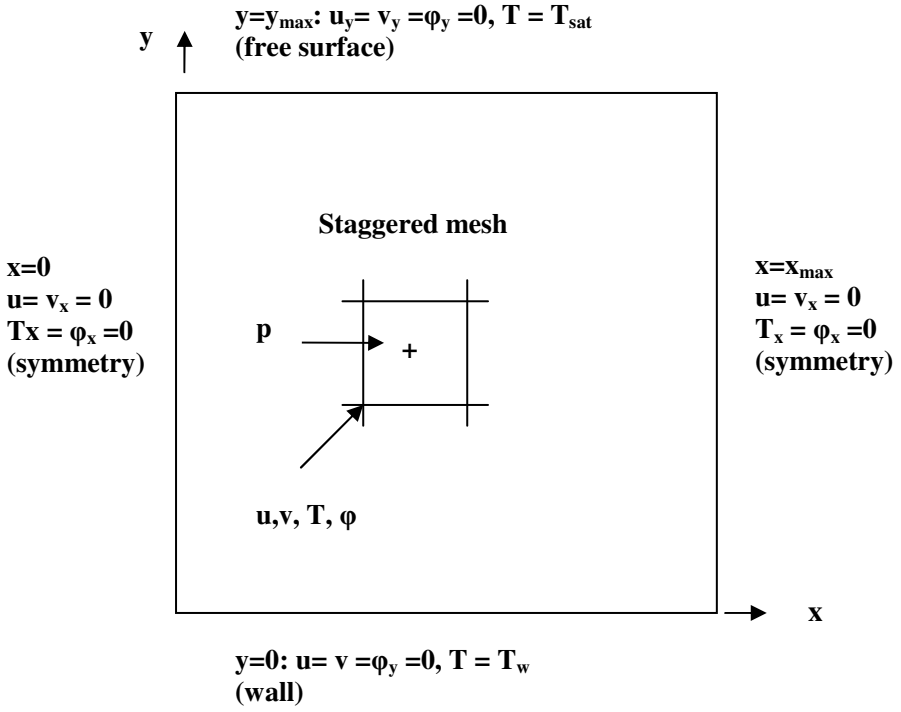

Fig. 2. Boundary conditions and the location of the variables stored in the staggered grid system

2.4 Numerical solution

The governing equations Eq. (1), (2), (3), (7) and (8) combined together are highly nonlinear. The equations are discretized using the finite difference method on a staggered grid system in which all the variables except pressure are stored at the grid points; pressure alone is stored at the cell center as shown in Fig. 2. The diffusion terms are considered implicit and the convection and source terms are considered explicit in time. For spatial approximations all terms are considered using second order central difference method and a second-order ENO method described by Chang et al.(1996) is applied to the convection terms to prevent numerical oscillations. The

pressure and velocity are solved in a sequential manner by the procedure described in Selvam (1997). The discretized equations for momentum, energy and pressure are symmetric and are solved by the preconditioned conjugate gradient procedure (Ferziger and Peric, 2002) in an iterative form. The iteration is done until the average residue for each node is reduced to less than 10^{-9}. This amount of accuracy is needed because of the high density difference between the liquid and the vapor. After assuming initial position for distance functions, the equations are solved sequentially at each time-step in the following order:

1. Solve the momentum equations, Eq. (1) for velocities
2. Correct the velocity to take the pressure effect
3. Solve the pressure Poisson equation to satisfy continuity
4. Update the velocities to include the new pressure effect
5. Solve temperature equation Eq. (2)
6. Solve the distance function Eq. (7)
7. Reinitialize the distance function as per Eq. (8) and go to next time step

During the computation, time steps were chosen to satisfy the Courant-Fredreichs-Lewy (CFL) condition. This condition is defined mathematically as $\Delta t \leq \min (h/(|u|+|v|))$. This was done because of the explicit treatment of the convection terms and the condition that the numerical results should not change if the time steps are halved.

3. Results and Discussion

Lin and Ponnappan (2003) conducted spray cooling experiments with FC-72 as the working fluid. At 101 kPa, FC-72's has a saturation temperature of T_{sat}=53˚C. The present effort was based on these saturation conditions, thus leading to the following reference values: l_r=736.2, u_r=85 mm/s, t_r=8.66 ms, and ΔT=10˚C. Other parameters of interest include: Re = 218, We = 1.0, Pe = 2050, Ja = 0.127, and ρ_l/ρ_v=138. For this study, these values were used with the exception of the density ratio, ρ_l/ρ_v = 20 which is similar to the value used by Selvam et al. (2005b). The density ratio is kept low to prevent numeric instability and reduce calculation time. Selvam et al. (2005b) noted that higher density ratios show a trend similar to lower density ratios, but the time steps needed for stable growth are much smaller, and are not explored in the current study.

3.1 Modeling Vapor Bubble Growth

For the initial study, a growing vapor bubble is considered. This case uses a domain of 0.4 units (294.5μm) and an initial bubble radius of 0.2 units (147.2μm) to reflect the heat transfer occurring at the die edges. The die edges are where droplet impingement and vapor merger would occur less frequently thus making nucleate boiling the primary means of heat transfer for this region. A 101 x 101 grid domain was used. This corresponded with a characteristic length for a single grid of 1.46μm.

These simulations provided data similar to that of nucleate boiling studies which have been previously studied experimentally and numerically by Dhir et al. (1998). The time step used in

the study by Dhir et al.(1998) was $2x10^{-5}$ units (173ns). This time step is larger than that used by Selvam et al.(2005b) and Selvam et al.(2005d). However, selection of the current time step was necessitated by the larger domain and relative slow speed of vaporization in the model for $\Delta T=10^{\circ}C$ (this still obeyed the CFL condition). Results for 1.0g and 2.0g were very similar, therefore only the 1.0g case is presented. Nu, $\overline{Nu}$, and velocity graphs for these micro scale interactions are given in Figs. 3(a&b), and Figs. 4(a&b) and 5(a&b) show vector plots for the liquid and vapor phases respectively.

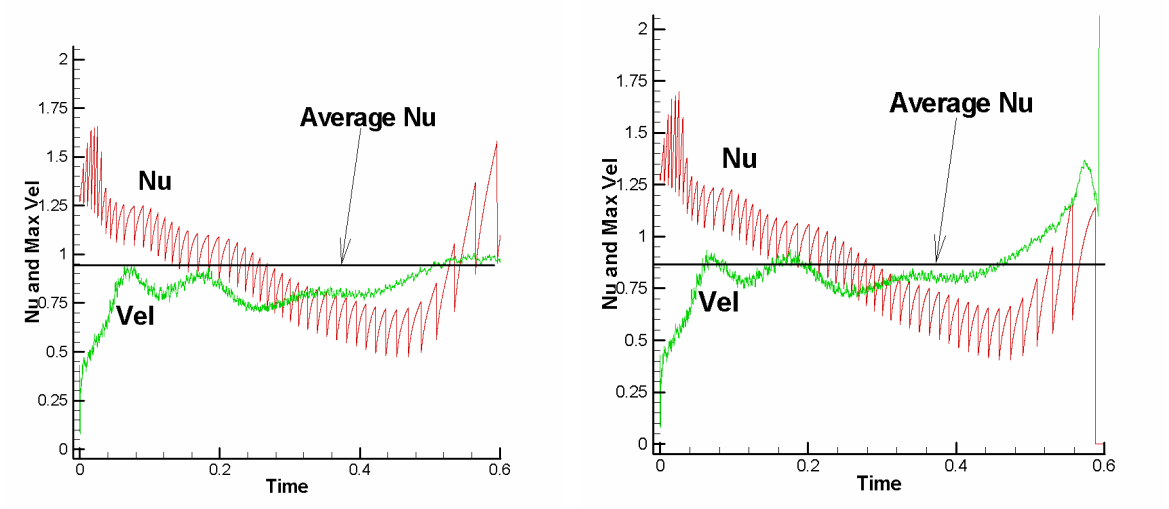

(a) 1.0g (b) 0.0001g

Figures 3 (a & b): Nu and Max Velocity for 1.0g and 0.0001g

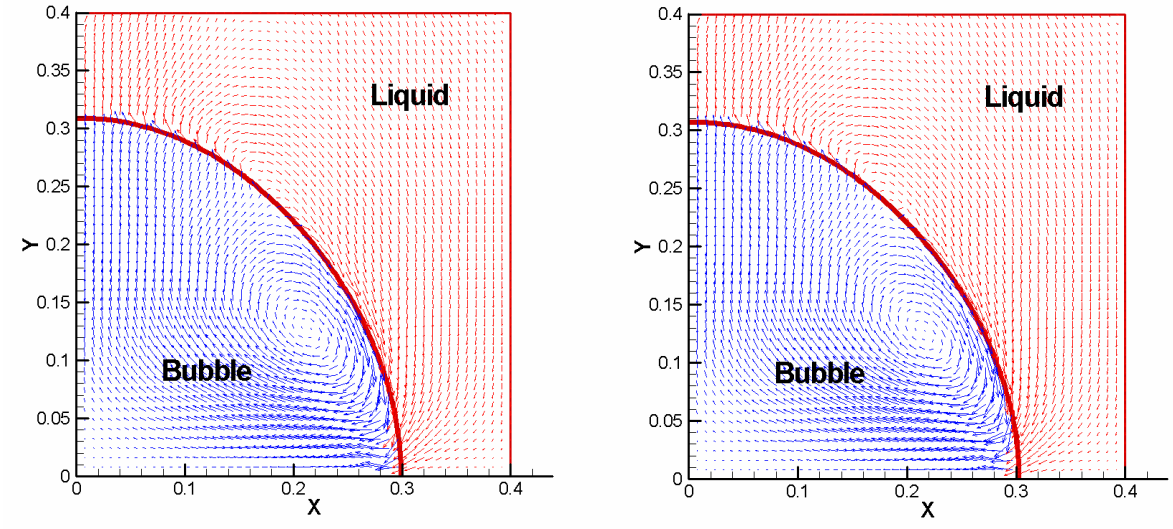

(a) 1.0g (b) 0.0001g

Figures 4 (a & b): Liquid-Vapor Vector Diagram Snapshots at 2.19ms for 1.0g and 0.0001g

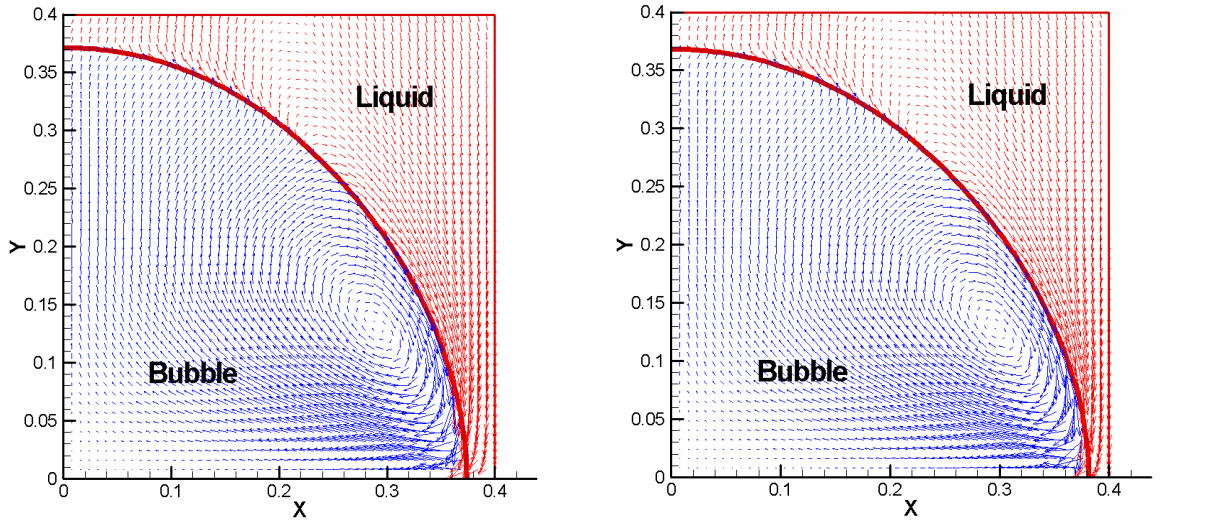

(a) 1.0g (b) 0.0001g

Figures 5 (a & b): Liquid-Vapor Vector Diagram Snapshots at 4.38 ms for 1.0g and 0.0001g

The growth rate and shapes of the bubbles didn't change significantly with gravitational variation. At time 4.38 ms (Fig. 5a & 5b), the size of the bubbles are 3.75 by 3.65 units^2 for 2.0g, 3.70 by 3.75 units^2 1.0g, and 3.7 by 3.8 units^2 for 0.0001g. There is a slight difference in aspect ratio between the 2.0g and 1.0g cases. In the 2.0g case, the bubble grown is slightly taller and narrower. However, in the 1.0g and 0.0001g cases, the bubbles were very similar. Nu peaked for all cases at $t=0.04t_r$ (346μs), which corresponds with the initial formation of the convective cell created by liquid evaporation at the wall. This is denoted by the velocity vortex near the wall. This vortex is an artifact of initial parameters selected in the model for the starting size of the vapor bubble and the initial velocity condition (initially set to zero throughout the domain). Nu rose sharply at $t=0.04t_r$ (346μs) to reflect the onset of this transient convection, but decreased once the velocities stabilized. Since the maximum Nu for these cases was influenced by the afore-mentioned initial conditions, the comparison of heat transfer for this case will be based on time-averaged $\overline{Nu}$ for each case rather than the maximum Nu. These averages were 0.943, 0.987, and 0.8881 for the 2.0g, 1.0g, and 0.0001g cases, respectively. The two modes of heat transfer occurring throughout the simulation are vaporization of the liquid and conduction through the liquid. The average heat transfer for the 0.0001g case was lower than the 1.0g and 2.0g cases because the large bubble created a barrier for the liquid path to the heater surface, thereby limiting the amount of conduction. The heat transfer for the 2.0g case was only slightly lower then the 1.0g, and is due to the 2.0g bubble interacting with the upper boundary of the computational domain, which had a free-surface condition. This coupling was not expected prior to runtime. Nonetheless, future work will be directed towards investigating this issue.

The previously mentioned study by Dhir et al. (1998) used a larger domain over which bubble growth and fluid dynamics were investigated in comparison to that used for the first part of this study. In order to compare the present model's results with the work of Dhir et al. (1998) growth phenomena for a large domain bubble size was also studied. A 2 unit (1.47mm) domain was used, with an initial bubble radius of 1 unit (0.74mm). This discretized grid mesh was 201 x

201 units, thus creating grid sizes of 7.31μm. A time step of $6x10^{-5}$ unit (52ns) was used for 16000 iterations, creating an overall time interval of 832μs. Figures 6(a&b) show the Nu and maximum velocity while figures 7(a&b) and 8(a&b) show the time evolution of the velocity vectors for 438μs and 788μs respectively. For comparison purposes, the 2.0g and 0.0001g cases are presented in figure form to more clearly show buoyant mechanisms.

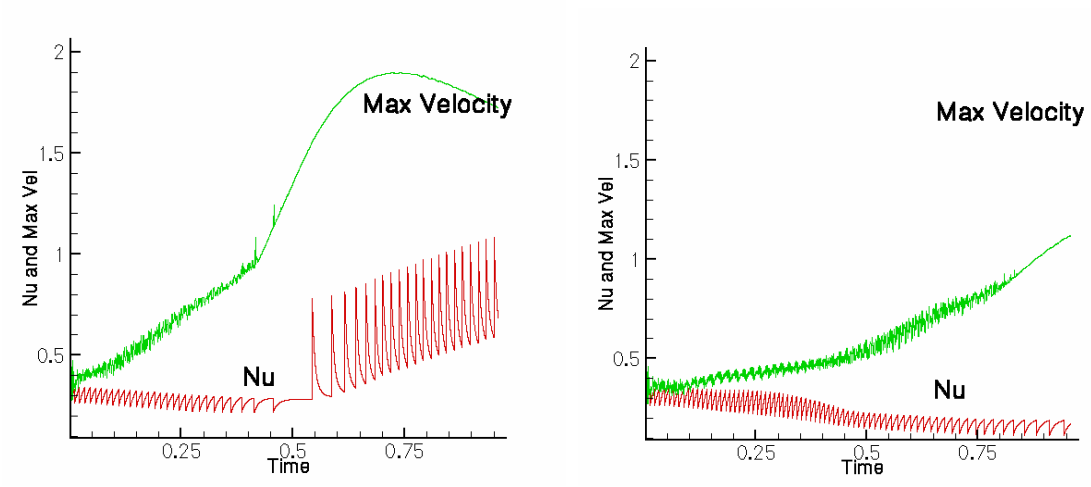

(a) 2.0g (b) 0.0001g

Figures 6(a &b): Nu and Max Velocity for 2.0g and 0.0001g

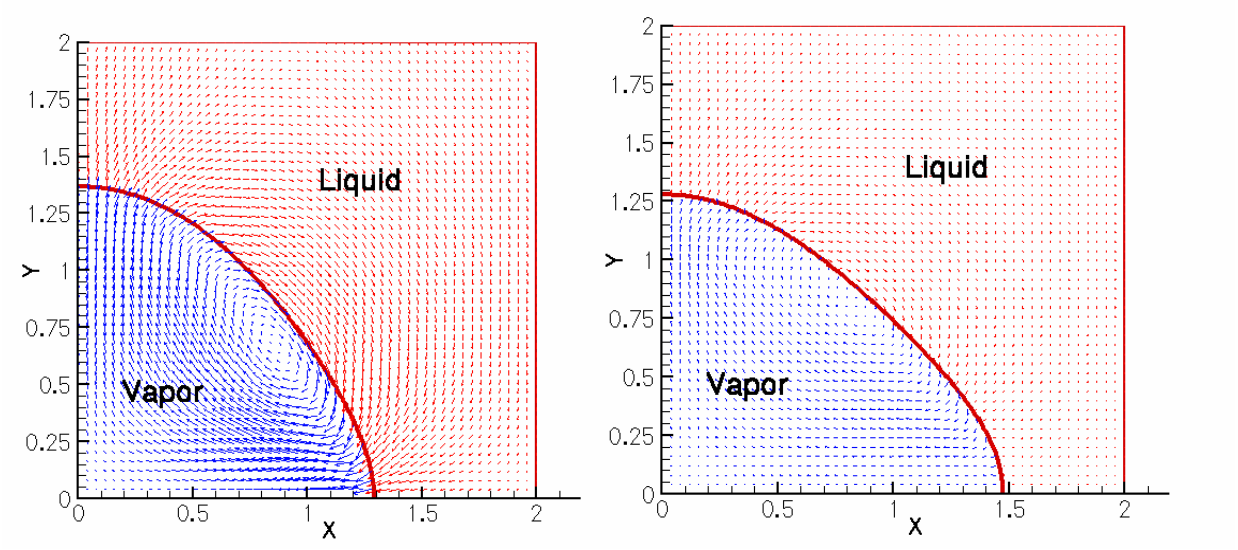

(a) 2.0g (b) 0.0001g

Figures 7(a & b): Liquid-Vapor Vector Diagram Snapshots at 438μs for 2.0g and 0.0001g

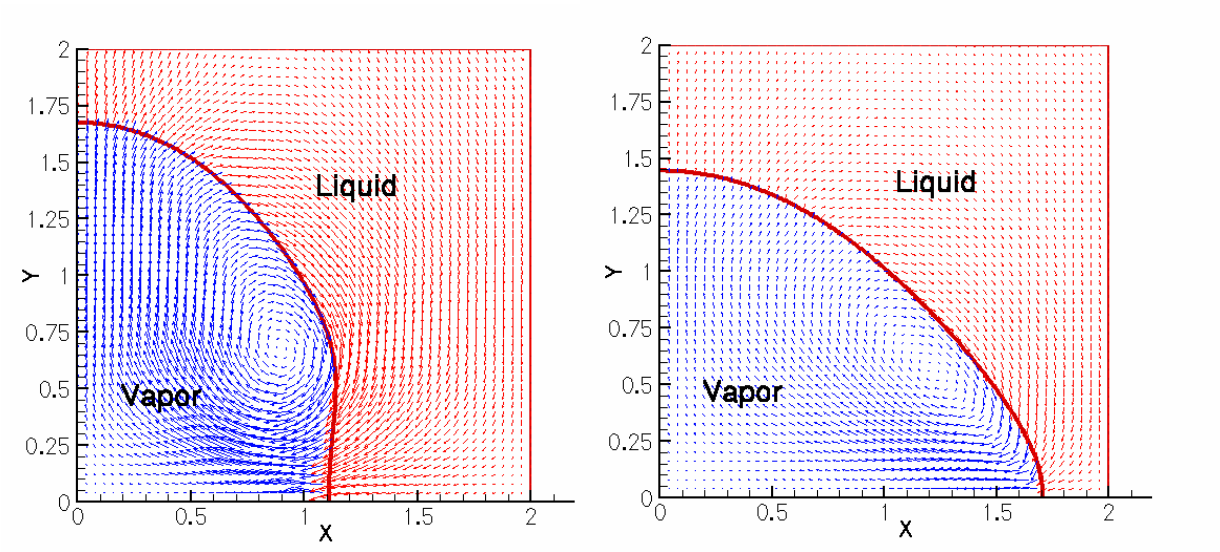

(a) 2.0g (b) 0.0001g

Figures 8(a & b): Liquid-Vapor Vector Diagram Snapshots at 788μs for 2.0g and 0.0001g

In this case, Nu decreases as the amount of liquid in contact with the hot wall decreases and the bubble grows. At $t=0.543t_r$ for the 2.0g and $t=0.820t_r$ for the 1.0g case, the Nu spikes and oscillates at this increased amplitude as shown by the latter half of Fig. 6a. This corresponds to the start of vapor bubble departure from the heater surface, which in Fig. 8a is seen as the bottom of the bubble pinch inward in preparation for wall separation. As the vapor bubble detaches, the liquid/solid contact area increases allowing for more heat transfer via conduction. This increase in Nu continued to rise as the bubble completely detached from the surface. This feature is notably absent from the 0.0001g case, where the bubble continues to grow. This growth is similar to that described in Dhir et al.(1998), who found that in reduced gravity the bubble tended to grow in an oblong sphere shape and had a much larger separation diameter then its normal gravity equivalent. Dhir's work, as well as the results presented show that the primary effect of reducing gravity is to reduce the buoyant forces that tend to lift the bubble off the wall, meaning surface tension and viscosity play much more significant role in microgravity.

Dhir et al. (1998) performed numerical and experimental work on the gravitational effects upon water in nucleate boiling. Their study showed that the gravity case took 0.25 seconds to grow a bubble to a size of 6.2mm (critical diameter). For the microgravity case, bubble growth to the critical diameter (209 mm) and departure from the heater surface only took 135 seconds and grew to a diameter of 209mm. This implies that in order to achieve bubble departure for the microgravity case, a significantly increased amount of computational time and space would be necessary because of the reduced buoyant effects. Since the liquid film thickness for spray cooling heat transfer is much smaller than the critical diameter previously reported, nucleate boiling alone is no longer applicable; bubble merger with a vapor region must also be considered for the thin film, and in spray cooling the film thickness is much smaller then the microgravity separation diameter. Future work is needed to determine what effects thick film simulations may have on spray cooling.

From the study of bubble growth in thin liquid film and pool boiling, it is clearly demonstrated that in thin liquid film (147.2 μm bubble radius) the effect of gravitational variation has little influence on bubble growth and associated heat transfer. This is due to the high surface tension effect in 147.2 μm bubble radius or less. The effect of micro and macro gravity effect on 0.74 mm bubble radius showed the difference in heat transfer and growth in bubble size. This verifies the model's capability to simulate the difference in bubble growth.

3.2 Modeling Thin Film Bubble Growth and Vapor Merger

For the thin film case, a bubble with a radius of 66.3μm was positioned at the origin of a 0.1 unit (73.6μm) thick liquid layer. This bubble was allowed to grow and merge with the vapor layer above it. The computational domain used was 0.4 x 0.4 units^2 (294.4μm^2). This was discretized by a 101 x 101 grid, which created grid sizes of 2.92 μm. A time step of 5x10^{-6} (43.3ns) was used for 40000 iterations, giving a total time interval of 1.73 ms. A similarity between the 2.0g and 1.0g cases allowed the 2.0g results to be omitted. Nu and $\overline{Nu}$ were recorded as well as the maximum velocity. These results are shown in Figs. 9(a&b). Vector plots for these cases at two instances (t=0.032t_r and t=0.064t_r) are given in Figs. 10-11(a&b).

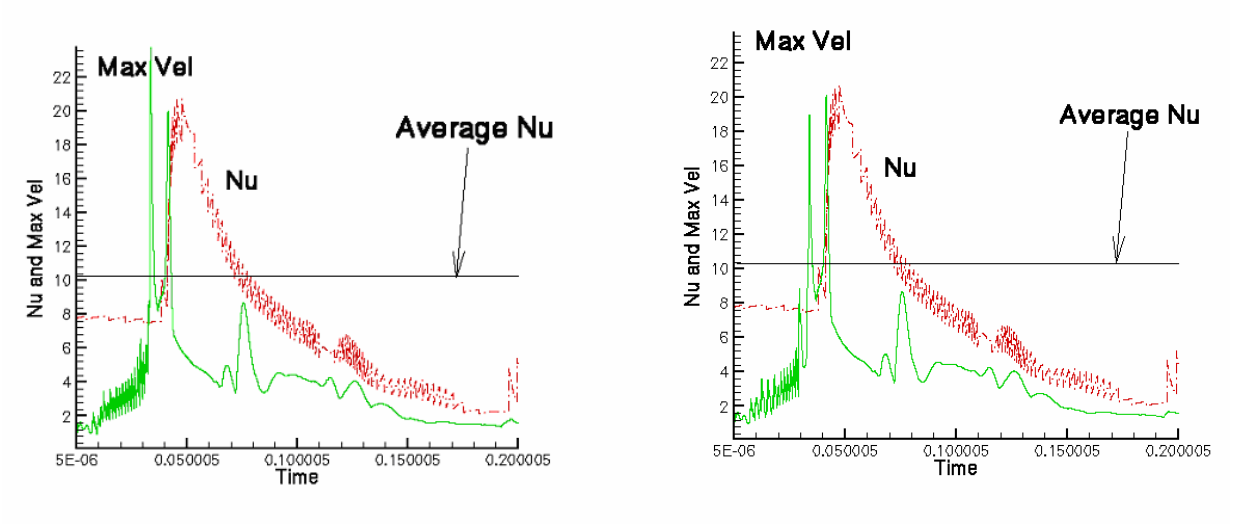

(a) 1.0g (b) 0.0001g

Figures 9(a & b): Nu and Max Velocity for 1.0g and 0.0001g

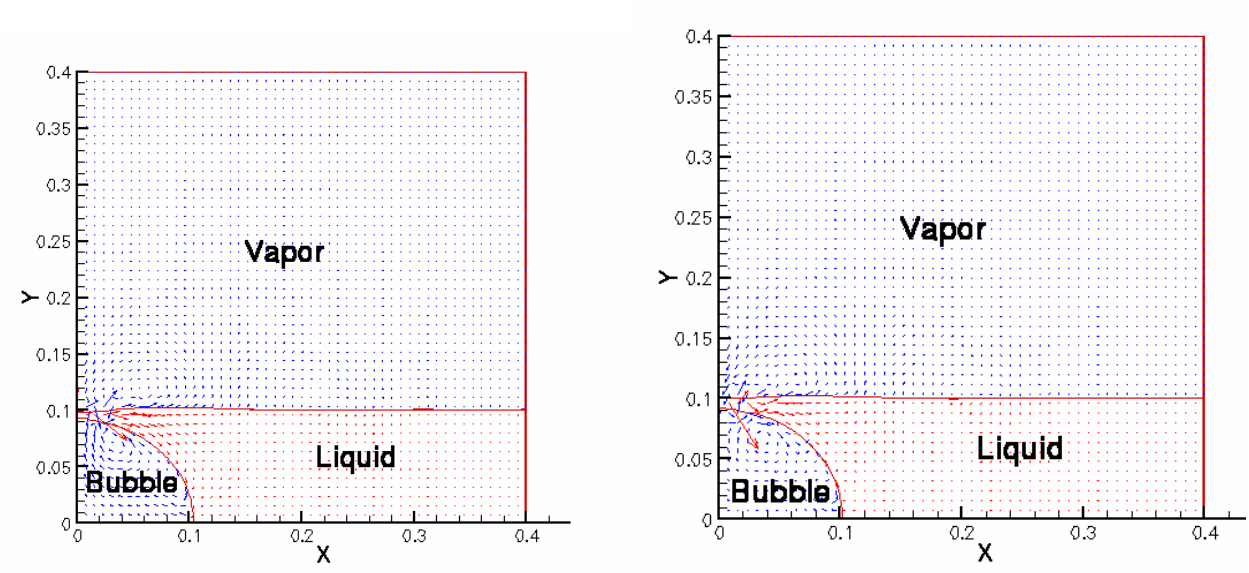

(a) 1.0g (b) 0.0001g

Figures 10(a & b): Liquid-Vapor Vector Diagram Snapshots at 273μs for 1.0g and 0.0001g

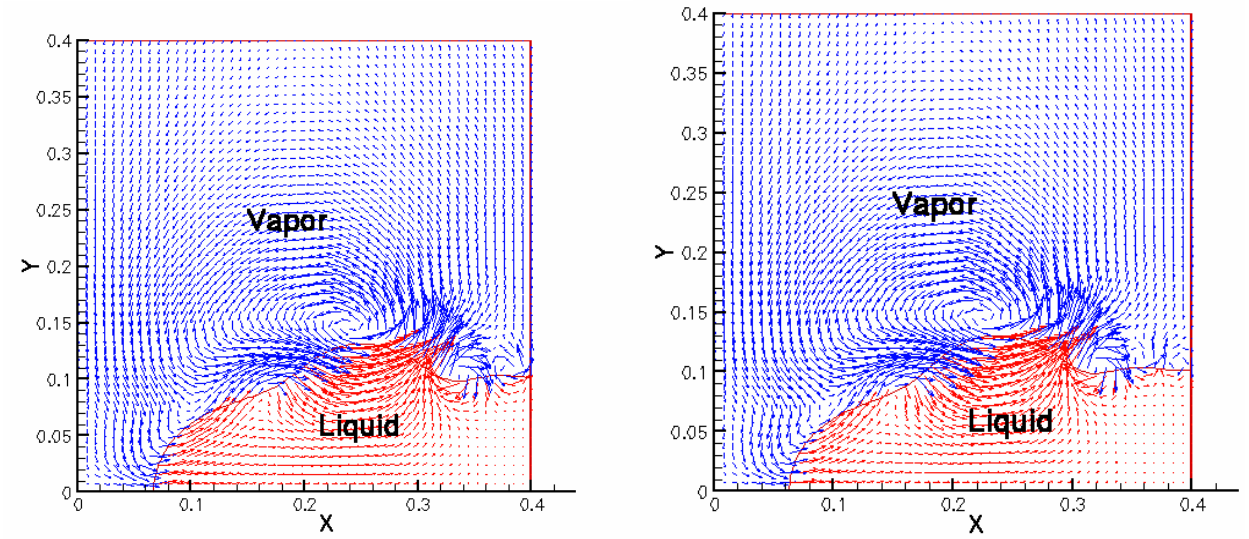

(a)1.0g (b) 0.0001g

Figures 11(a & b): Liquid-Vapor Vector Diagram Snapshots at 547μs for 1.0g and 0.0001g

The $\overline{Nu}$ for cases 2.0g, 1.0g, and 0.0001g were 10.307, 10.303, and 10.302, respectively. The maximum variation between these values was 0.0004%. The peak Nu occurred for all cases when the vapor bubble merged with the vapor layer above it. This was found to occur at each of the following: Nu= 20.661 at t=0.047000t_r (407μs) for the 2.0g case, Nu=20.733 at t=0.047585t_r (412μs) for the 1.0g case, and Nu=20.711 at t =0.047380t_r (410μs) for the 0.0001g case. As with the time-averaged values, these cases have a variation much less than 1%. The peak in Nu corresponds closely with the peak in maximum velocity for each case. As noted previously, this occurred when the vapor bubble merged with the vapor at the liquid/vapor interface. Therefore,

one may conclude the peak in heat transfer is due to the increased movement of the system, which allowed the liquid to replace the vapor along the heated wall. Selvam et al.(2005b) found similar results for a gravitational reference frame of 1.0g. A more detailed analysis pertaining to this case may be found in that reference.

3.3 Modeling Droplet Impingement on Growing Bubble in Thin Film

For the droplet impingement case, a scenario very similar to that used in the vapor bubble vapor interface merger study was applied. The primary difference was that a droplet was added to the solution domain. The droplet had a radius of 0.06 unit (44.2μm) and was placed with its center 0.2 units above the film and 0.2 units to the right of the y-axis (as shown in Fig. 12). The y-axis is taken as the bubble center. It had an initial dimensionless velocity of 20 units downward (i.e. 1.7m/s). In the study by Selvam et al.(2004) a dimensionless unit velocity of 30 (2.56m/s) was used to more closely resemble the published experimental conditions (Baysinger et al. 2004). Selvam et al.(2004) used a 201 x 201 mesh to discretize their solution domain for droplet impingement. Due to time considerations, a 101 x 101 mesh was used to attain computational results in a time efficient manner. This meant that a lower droplet velocity had to be used to avoid numeric instabilities. Nonetheless, both Selvam et al. (2004d) and the current work agree that higher velocities will be instrumental in furthering the understanding of spray cooling phenomena, and should be investigated in future efforts. Only 1.0g and 0.0001g figures are displayed due to similarities between the 2.0g and 1.0g cases. Graphs of Nu and maximum velocities are give in Figs. 13(a&b). Figs. 14-15(a&b) show liquid/vapor velocity fields at times $t=0.1055t_r$ and $t=0.1583t_r$, respectively.

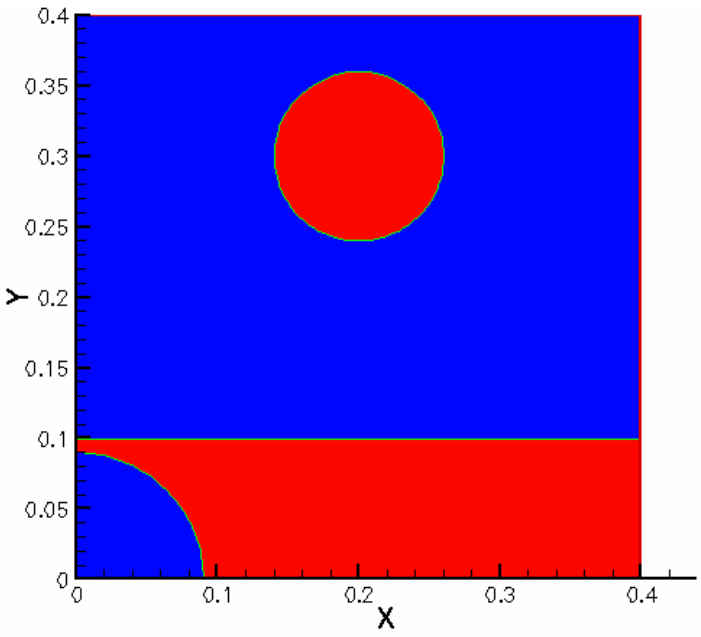

Fig.12 Droplet Impingement Configuration

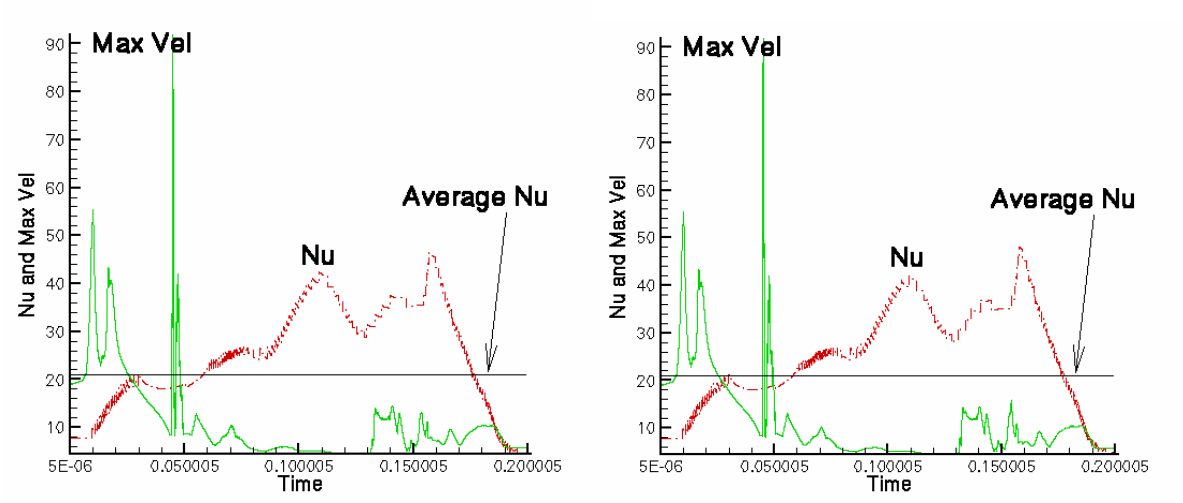

(a) 1.0g (b) 0.0001g

Figures 13 (a & b): Nu and Max Velocity for 1.0g and 0.0001g

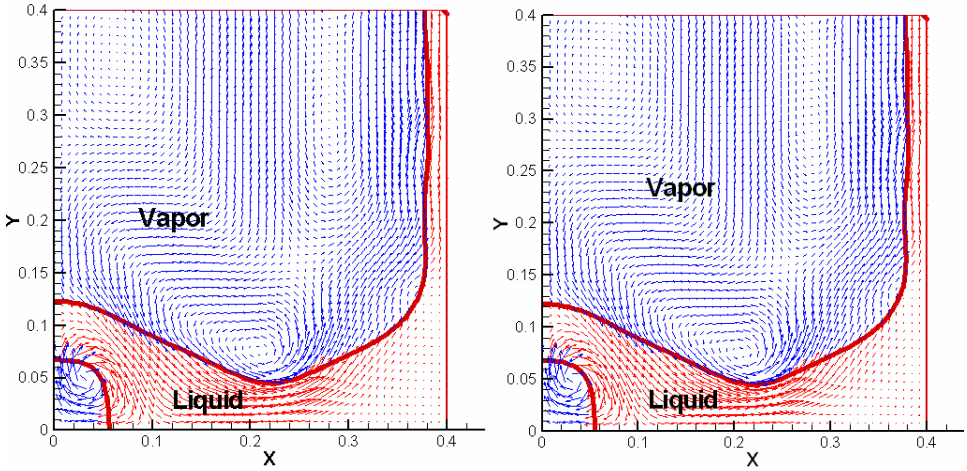

(a) 1.0g (b) 0.0001g

Figures 14 (a & b): Liquid-Vapor Vector Diagram Snapshots at 910μs for 1.0g and 0.0001g

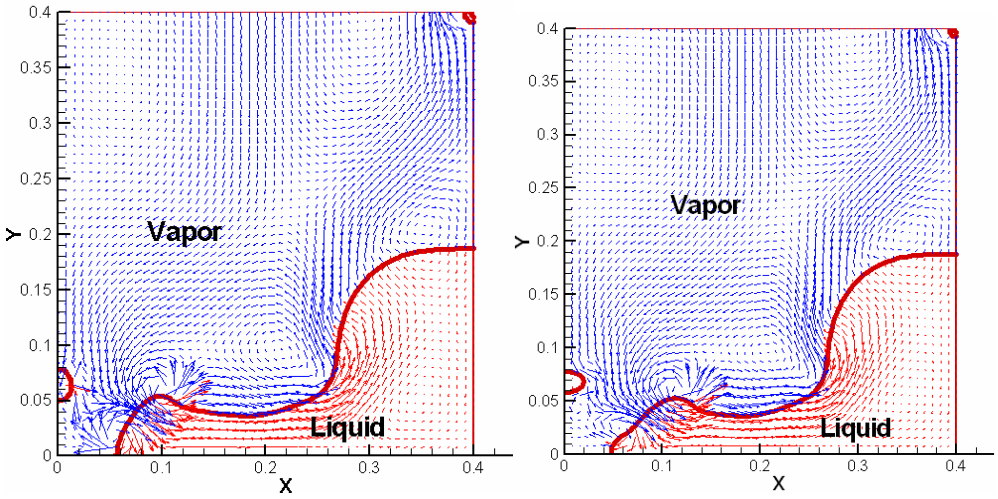

(a) 1.0g (b) 0.0001g

Fig Figures 15 (a & b): Liquid-Vapor Vector Diagram Snapshots at 1.37ms for 1.0g and 0.0001g

Results for the droplet impingement model showed two local maxima in Nu for each of the cases, occurring at similar times between varying gravity conditions. The first occurs when the cooled droplet displaces some of the bubble's vapor along the cool wall (shown in Fig.14 a&b) thus creating high transient conductive heat exchange. The values of Nu are 42.0 at t_r=0.108 (0.94ms) for the 2.0g case, 42.0 at t_r =0.109 (0.94ms) for the 1.0g case, and 41.1 at t_r =0.106 unit time (0.92ms) for the 0.0001g case. The second peak in Nu occurs when the cooled droplet, now completely merged with the liquid film, experiences a secondary contact with the hot wall, creating a large thermal gradient and producing higher heat flux. The values of Nu for the secondary contact are 47.9 at t_r =0.156 (1.35ms) for 2.0g, 48.1 at t_r =1.58 (1.37ms) for 1.0g, and 48.1 at t_r =1.58 (1.37ms) for 0.0001g (as shown in Fig. 15 a&b). This indicates that higher heat fluxes are achieved when cooler liquid contacts the hot wall directly as opposed to steadily conducting through the liquid film to a cooler surface temperature maintained by droplet impingement, similar to the findings in the study by Selvam et al.(2005b) and is in agreement with physical theory, specifically Fourier's law of heat conduction and Newton's law of cooling. Of prime importance to this study is the fact that the transient conduction, which accounts for the majority of droplet impingement heat transfer in Selvam et al.(2005b) is seemingly not dependant on gravitational variation.

4. Future Work

The actual liquid-vapor density of FC-72 is much larger (6 times) than the value used in this study. The lower density ratio was used because of its similarity to higher density ratios for tested cases (Selvam et al.2005b), and allowed for a significant reduction in computational time. Another factor similar in nature to density ratio is the droplet velocity. The value used in this and previous numerical studies on spray cooling (Selvam and Ponnappan 2004;Selvam et al. 2005b, 2005c, and 2005d) have all been lower then the experimental droplet velocity, according to Selvam et al.(2005b). Chen et al.(2002) showed that droplet velocity was the dominant variable in determining critical heat flux, and that CHF increased with increasing velocity. Future investigations are required to determine if higher velocities have a significant impact on heat transfer on the single droplet level of interaction investigated here and in Selvam et al.(2005b).

Two future studies currently under consideration are investigating the effects of subcooled liquid and thick liquid film interactions on spray cooling. Most heat transfer processes incorporate subcooling. Thus, the subcooling effect upon spray cooling is a topic of interest. The thick liquid film study also is of interest. In the study by Pautsch et al. (2004), the liquid film thickness is highly dependant upon the volumetric flow rate. Furthermore, the liquid film thickness increased as flow rate was decreased. Since failure mode effects are of prime importance to the applicability of spray cooling systems, a study of the thick liquid film case would give some idea as to heat transfer that can occur during a soft failure of a spray cooling system.

5. Conclusions

1. For the small scale vapor bubble growth model, it was shown that gravity does not play a significant role in heat transfer. The maximum variation between gravity cases (1.0g and 0.0001g) provided a difference in $\overline{Nu}$ of 10%. It was also shown that the convective cell

and vaporization of the liquid were the primary means of heat transfer. Neither of these phenomena were seen to exhibit significant differences under varying gravitational reference frames.

2. For the case of the large scale vapor bubble with growth, gravity dependence was observed in the model. In this case the primary means of heat transfer was vaporization along the wall at the interface of the bubble and liquid as well as transient conduction due to localized fluid motion. This motion was primarily due to bubble departure. Thus heat transfer for large scale vapor bubble growth is dependant on both buoyancy and gravitational forces.
3. For the bubble to liquid/vapor interface merger case, the maximum Nu occurred due to transient conduction caused by the movement of the bubble when bursting. This allowed cooler liquid to come into contact with the heater surface, thereby increasing the thermal gradient at the wall. Peak Nu varied between gravitational constants a maximum of 0.3%. On the length scale considered, surface tension as opposed to gravitational forces had the dominant effect upon fluid motion and heat transfer.
4. In the droplet impingement case, the heat transfer was not affected significantly by gravity. The factors that provided an increase in heat transfer compared to the bubble merger case were a result of relatively cooler ($T=T_{sat}$) droplet impingement at the liquid/vapor interface. The perturbation through the liquid film initiated during droplet contact with the liquid/vapor interface allowed for a larger amount of liquid motion than in the vapor bubble to liquid/vapor interface merger case. In addition, the localized cooling effect created by the droplet provided a larger thermal gradient between the localized liquid and the heater surface. This instituted greater heat transfer, and was varied only 2% between gravitational constants.
5. The bubble growth and vapor merger and droplet impingement modeling studies are part of the spray cooling phenomena. From the study we could conclude that the gravitational variation has little effect on heat transfer.

6. Acknowledgements

This work was made possible by an SBIR grant from the NASA Goddard Space Center, funded through PELS, L.L.C and the University of Arkansas, Fayetteville. The work was performed at the Computational Mechanics Laboratory at the U of A, and is the charge of Dr. Selvam.

References

1. K.M. Baysinger et al. (2004), Design of a Microgravity Spray Cooling Experiment, AIAA-2004-0966, 42nd AIAA Aerospace Sciences Conference, Jan. 5-8, Reno, NV.
2. J.U. Brackbill, D.B. Kothe and C. Zamach (1992), A continuum method for modeling surface tension, *J. Comp. Physics*, 100, 335-354.
3. E. Cabrera and J.E. Gonzalez (2003), Heat flux correlation for spray cooling in the nucleate boiling regime, *Exp. Heat Transfer*, 16, 19-44.
4. Y.C. Chang, T.Y. Hou, B. Merriman and S. Osher (1996), A level set formulation of Eulerian interface capturing methods for incompressible fluid flows, *J. Comp. Physics*, 124, 449-464.
5. R.H. Chen, L.C. Chow, J.E. Navedo, Effects of Spray Characteristics on Critical Heat Flux in Subcooled Water Spray Cooling, *Int. J. of Heat and Mass Transfer*, 45, 4033-4043.

6. L.C. Chow, M.S. Sehembey and M.R. Paris (1997), High heat flux spray cooling, *Ann. Rev. Heat Transfer*, 8, 291-318
7. V.K. Dhir, D.M. Qiu, N. Ramanujapu, and M.M. Hasan (1998), Investigation of Nucleate Boiling Mechanisms Under Microgravity Conditions, *Proceedings of the Fourth Microgravity Fluid Physics and Transport Phenomena Conference*, Cleveland, OH, 1998.
8. J.H. Ferziger and M. Peric (2002), *Computational Methods for Fluid Dynamics*, Springer, New York
9. C.A. Hunnell, J.M. Kuhlman, and D.D. Gray (2006), Spray Cooling in Terrestrial and Simulated Reduced Gravity, *Proceedings of the Space and Technology Applications International Forum (STAIF 2006)*, Albuquerque, NM, Feb. 11-14.
10. L. Lin and R. Ponnappan, (2003), Heat transfer characteristics of spray cooling in a close loop, *Int. J. Heat Mass Transfer*, 46, 3737-3746
11. I. Mudawar (2001), Assessment of high heat-flux thermal management schemes, *IEEE Transactions on Components and Packaging Technologies*, 24, 122-141
12. S. Osher and R. Fedkiw (2003), *Level set methods and dynamic implicit surfaces*, Springer, New York. Applies Mathematical Sciences: Vol. 153.
13. A.G. Pautsch and T.A. Shedd (2005), Spray impingement cooling with single- and multiple-nozzle arrays part 1: heat transfer data using FC-72, *Int. J. of Heat and Mass Transfer*, 48, 15, 3167-3175.
14. A.G. Pautsch, T.A. Shedd and G.F. Nellis (2004), Thickness Measurements of the Thin Film in Spray Evaporative Cooling, *2004 Inter Society Conference on Thermal Phenomena***,** 70-76
15. D.M. Qiu and V.K. Dhir (2002), Single-Bubble dynamics During Pool Boiling Under Low Gravity Conditions, *Journal of Thermophysics and Heat Trnasfer*, Vol. 16, No.3, Sept. 2002.
16. B.L. Rowden, R. P. Selvam, E.A. Silk (2006), Spray Cooling Development Effort for Microgravity Environments, *AIP Conference Proceedings* Vol.: 813, pp 134-144, American Institute of Physics, Ed. M.S. El-Genk, *Proceedings of the Space and Technology Applications International Forum (STAIF 2006)*, Albuquerque, NM, Feb. 11-14.
17. R. P. Selvam (1997), Computation of pressures on Texas Tech building using large eddy simulation, *J. Wind Engineering and Industrial Aerodynamics*, 67 & 68, 647-657.
18. R.P. Selvam and R. Ponnappan (2004), Numerical modeling of nucleation boiling in thin film and effect of droplet impact, *Proceedings of the 15th Annual Thermal & Fluids Analysis Workshop (TFAWS 2004)*, Pasadena, CA, Aug. 30th to Sep. 3rd.
19. R.P. Selvam, L.Lin and R. Ponnappan (2005a), Computational modeling of spray cooling: Current status and future challenges, *AIP Conference Proceedings* Vol.:746, pp 56-63, American Institute of Physics, Ed. M.S. El-Genk, *Proceedings of the Space Technology and Applications International Forum (STAIF 2005)*, Conference on Thermophysics in Microgravity, Albuquerque, NM, Feb. 13-17
20. R.P. Selvam, L. Lin and R. Ponnappan, (2005b), Direct Simulation of Spray Cooling: Effect of Vapor Bubble Growth and Liquid Droplet Impact on Heat Transfer, paper accepted by *The International Journal of Heat and Mass Transfer*.
21. R.P. Selvam, S. Baskara, J.C. Balda, F. Barlow and A. Elshabini (2005c), Computer Modeling of Lquid Droplet Impact on Heat Transfer During Spray Cooling, *Proceedings of the 2005 ASME Summer Heat Transfer Conference, paper no: HT2005-72569*, San Francisco, CA, July 17-22.

22. R.P. Selvam, M. Sarkar, and R. Ponnappan (2005d), Modeling of Spray Cooling: Effect of Droplet Velocity and Liquid to Vapor Density Ratio on Heat Transfer, *Proceedings of the 16th Annual Thermal & Fluids Analysis Workshop (TFAWS 2005)*, Orlando, FL, Aug. 8-12.
23. J.A. Sethian (1999), *Level set methods and fast marching methods: Evolving interfaces in computational geometry, fluid mechanics, computer vision and materials science*, Cambridge University Press, Cambridge, UK.
24. G. Son, and V.K. Dhir (1998), Numerical simulation of film boiling near critical pressures with a level set method, *Journal of Heat Transfer*, 120, 183-192.
25. G. Son, N. Ramanujapu and V.K. Dhir (2002), Numerical simulation of bubble merger process on a single nucleation site during pool nucleate boiling, *Journal of Heat Transfer*, 124, 51-62.
26. M. Sussman, P. Smereka and S. Osher, (1994), A level set approach for computing solutions to incompressible two-phase flow, *J. Comp. Physics*, 114,146-159.
27. J. Yang, L.C. Chow and M.R. Paris (1996), Nucleate boiling heat transfer in spray cooling, *Journal of Heat Transfer*, 118, 668-671

Nomenclature

c_p	specific heat at constant pressure
Fr	Froude number
g	gravity vector
H	step function
h	grid spacing
h_{fg}	latent heat of evaporation
Ja	Jacob number = $c_{pl} \Delta T / h_{fg}$
k	thermal conductivity
l_r	characteristic length $\sqrt{\sigma/g(\rho_l - \rho_v)}$
m	mass flux vector
Nu	Nusselt number $q\, l_r /(\Delta T\, k_l)$
$\overline{Nu}$	time-averaged Nu
p	pressure
Pe	Peclet number = $\rho_l\, u_r\, l_r\, c_{pl} / k_l$
Pr	Prandtl number = $c_{pl}\, \mu_l / k_l$
q	heat flux
Re	Reynolds number = $\rho_l\, u_r\, l_r / \mu_l$
T	temperature
T^*	dimensionless temperature $(T-T_{sat})/(T_w-T_{sat})$
ΔT	temperature difference $T_w - T_{sat}$
t	time
t_r	characteristic time l_r / u_r
u	velocity vector (u,v)
$\mathbf{u}_{int}$	interface velocity vector
u_r	characteristic velocity $\sqrt{g l_r}$
We	Weber number = $\rho_l\, u_r^2\, l_r / \sigma$
α	thermal diffusivity
κ	interfacial curvature

μ	dynamic viscosity
ρ	density
σ	surface tension
φ	level set function

Subscripts

int	interface
l, v	liquid , vapor
sat, w	saturation, wall